CrossMark

ORIGINAL PAPER

The Transition from Transient Oxide to Protective Al$_2$O$_3$ Scale on Fe–Cr–Al Alloys During Heating to 1000 °C

Suzue Yoneda[1] · **Shigenari Hayashi**[1] ·
Shigeharu Ukai[2]

Abstract The transition behavior of an Al-rich amorphous oxide layer to an external Al$_2$O$_3$ layer on Fe–(4, 24)Cr–(6, 10)Al (at.%) alloys was investigated during heating to 1000 °C at a heating rate of 50 °C/min, by means of in situ high-temperature X-ray diffraction measurement and TEM observation. In the alloy containing 6Al, internal amorphous Al$_2$O$_3$ was initially developed below the Al-rich amorphous surface layer. The amorphous internal precipitates transformed to be crystalline and grew laterally with time. The internal precipitates subsequently connected with each other to form a continuous α-Al$_2$O$_3$ scale. In the case of 10Al alloy, an Al-rich amorphous layer transitioned to a crystalline α-Al$_2$O$_3$ layer from the interface between transient/amorphous layers during heating. The Al$_2$O$_3$ scale developed on high Al alloys contained Fe and Cr with relatively higher contents, but that formed on low Al alloy contained low Fe and Cr. The effect of Cr on promoting an external Al$_2$O$_3$ scale formation was found to be weaker for alloys with higher Al content compared to the alloys with lower Al content, if Al$_2$O$_3$ scale was directly transitioned from the amorphous layer.

Keywords Transient oxidation · Al$_2$O$_3$ scale · Amorphous oxide · Internal oxidation

✉ Suzue Yoneda
s.yoneda@frontier.hokudai.ac.jp

1 Department of Metallurgy and Ceramics Science, Graduate School of Science and Engineering, Tokyo Institute of Technology, 2-12-1-S8-3, Ookayama, Meguro-ku, Tokyo 152-8552, Japan

2 Division of Materials Science and Engineering, Faculty of Engineering, Hokkaido University, N13 W8, Kita-ku, Sapporo 060-8628, Japan

Introduction

During the initial oxidation stage at higher temperatures, high-temperature oxidation resistant alloys usually form various transient oxides, such as Fe-, Ni-, Al-, Cr-rich oxides. The oxidation stage then transitions to a steady-state stage where a protective oxide scale such as Cr_2O_3 or Al_2O_3 forms below the transient oxides by selective oxidation of Cr or Al. In the steady-state oxidation stage, the alloys are protected from high-temperature oxidizing environments by the stable protective oxide scale.

The oxidation behavior of the alloys in the transient oxidation stage has been widely reported. In the case of the Al_2O_3 scale-forming alloys, the transient oxidation behavior contains various phenomena such as initial transient oxide formation and metastable to stable Al_2O_3 phase transformation. Golightly et al. [1] investigated the early stage of development of an Al_2O_3 scale on Fe–Cr–Al alloys at 1000 and 1200 °C. They reported that a steady-state oxide α-Al_2O_3 was established on Fe–14Cr–4wt%Al and Fe–27Cr–4wt%Al alloys after only a few minutes of oxidation at 1000 °C, and transient oxides rich in Fe and Cr were initially formed prior to α-Al_2O_3 scale formation. The important finding in their study is that the steady-state oxidation stage was established more rapidly for alloys with higher Cr contents and at higher temperatures. However, Kear et al. [2] reported that the transition to Al_2O_3 takes about 40 min on Ni–15Cr–6wt%Al at 1000 °C. Regarding the phase transformation of Al_2O_3 scale, Brumm et al. [3] reported that Cr in Ni–Al–Cr alloys accelerates the phase transformation from metastable θ-Al_2O_3 to α-Al_2O_3, and Cr_2O_3 nuclei serve as nucleation sites for α-Al_2O_3. Kitajima et al. [4] reported that Fe or Cr coating on Fe-50Al alloy accelerates the phase transformation from metastable θ-Al_2O_3 to α-Al_2O_3. These results suggest that the initial transient oxidation affects the subsequent phase transformation of Al_2O_3 scale.

In our previous studies [5, 6], we investigated the initial oxidation behavior by using Fe–xCr–6at.% Al ($x = 0$–24) alloys, which are relatively lower Al alloys comparing to commercial Fe–Cr–Al alloys such as Kanthal AF and MA956, containing about 10 at.%Al, during heating in order to clarify the effect of Cr on an external Al_2O_3 scale formation, and discussed the effect of Cr on promoting an external Al_2O_3 scale formation by in situ high-temperature X-ray diffraction analysis and TEM observation. Figure 1 shows a schematic of the effect of Cr on oxidation behavior of binary Fe–Al and ternary Fe–Cr–Al alloys during heating to 1000 °C. In this schematic, Fe–Cr alloy is also included in order to indicate the effect of Al. We found (1) An Al-rich amorphous oxide layer was found to develop below the outer Fe-rich transient oxide scale on Fe–Al and Fe–Cr–Al alloys at lower temperature. This Al-rich amorphous layer was found to act as a protective layer during heating up to about 800 °C until a protective Al_2O_3 scale was formed. Therefore, initial oxidation mass gain of Fe–Al alloy is much lower than that of Fe–Cr, and (2) Cr improved the long-term oxidation resistance of this amorphous layer by delaying the time for breakdown [6]. After heating to 900 °C, Al was internally oxidized below the amorphous layer in Fe–xCr–6Al alloy regardless of alloy Cr content, and (3) the volume fraction of internal Al_2O_3 increased with increasing
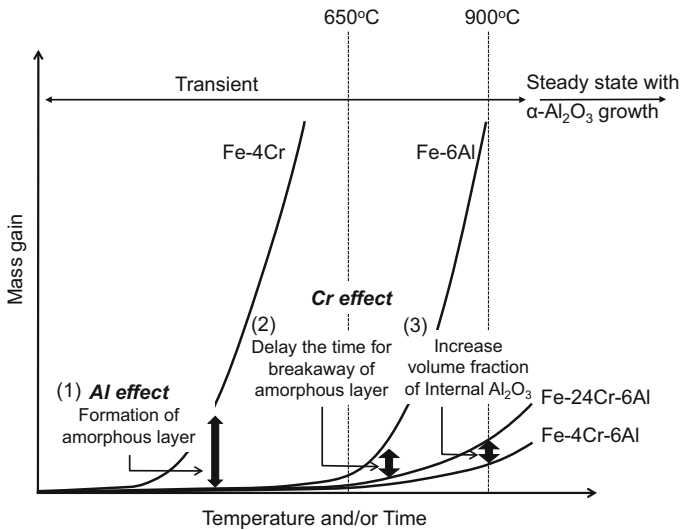
Fig. 1 Schematic of oxidation kinetics of binary Fe–Cr, Fe–Al and Fe–Cr–Al alloys during heating to 1000 °C with a heating rate of 50 °C/min

alloy Cr content which results in higher mass gain of alloys with higher Cr content, but may promote rapid transition to external Al_2O_3 scale. Finally, an external Al_2O_3 scale was developed and oxidation continued with a slower oxidation rate. The transition from Al-rich amorphous layer accompanied by internal Al_2O_3 to a protective Al_2O_3 scale formation occurred at temperatures between 900 and 1000 °C; However, the detail of transition behavior from internal to external Al_2O_3 scale was not clearly understood. Moreover, the effect of Cr on this transition phenomenon has not been clearly understood. Therefore, in this study, we investigated the detailed transition behavior by observing the change in the structure of internal precipitate until establishment of an external Al_2O_3 scale in order to understand the effect of Cr on Al_2O_3 scale formation in more detail. Additionally, we also investigated the direct transformation from an Al-rich amorphous to an external Al_2O_3 scale by using the alloys with higher Al content, ~ 10 at.%.

The purpose of this study is to investigate the process of the establishment of the protective Al_2O_3 scale and understand the effect of Cr and Al contents on Al_2O_3 scale formation by analysis of structural and microstructural developments of oxides during the heating stage, by means of in situ high-temperature X-ray diffraction measurement and TEM observation.

Experimental Procedures

Table 1 shows the alloy composition used in the present study. All alloys were prepared by argon arc melting using high-purity metals (99.99 at.%) as the starting constituents. The alloy ingots were then homogenized in vacuum at 1200 °C for

**Table 1** Nominal composition of the alloys used in present study

Fe (at.%)	Cr (at.%)	Al (at.%)
Bal.	4	6
Bal.	24	6
Bal.	4	10
Bal.	24	10

48 h. Approximately 1-mm-thick samples were cut from the homogenized ingots and ground to a 4000-grit finish using SiC abrasive paper. Samples were then polished using 3 μm diamond paste, followed by ultrasonic cleaning in acetone prior oxidation test.

In situ high-temperature X-ray diffraction measurement was performed at the beam-line BL19B2 of the SPring-8 at Japan Synchrotron Radiation Research Institute. Detailed experimental setup for in situ measurement is explained elsewhere [5]. The camera length between the two-dimensional X-ray detector and the sample surface was set to 438.31 mm. After setting up the apparatus, the sample was heated to 1000 °C in air at a heating rate of 50 °C/min, followed by isothermal oxidation for 30 min in air. During heating, isothermal oxidation and cooling, the diffracted signals from the sample surface were collected every 10 s, with a collection time of 6 s.

After oxidation testing, surface morphology was observed by scanning electron microscopy (SEM) and cross sections of the oxide scale were observed by transmission electron microscopy (TEM) and scanning transmission electron microscopy (STEM). Element distributions were analyzed by an energy dispersive X-ray spectrometer (EDS) attached to the STEM.

Fig. 2 Oxidation kinetics of binary Fe–6Al, Fe–xCr–6Al and Fe–xCr–10Al alloys during heating to 1000 °C with a heating rate of 50 °C/min. The data of Fe–6Al, Fe–4Cr–6Al, Fe–12Cr–6Al and Fe–24Cr–6Al are superimposed from Fig. 2 in Ref. [5]
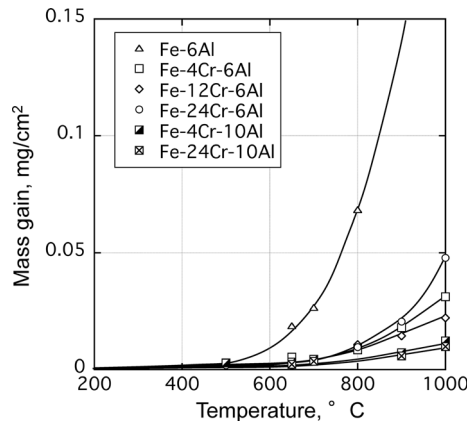
Results

Oxidation Kinetics

Figure 2 shows the oxidation kinetics of Fe–6Al and Fe–Cr–Al alloys with different Al and Cr contents during heating to 1000 °C. The oxidation mass gains of Fe–6Al and Fe–xCr–6Al in Fig. 2 were superimposed from our previous study [5]. Cr effect on oxidation performance of Fe–6Al alloy was very clear as discussed in our previous study; 4%Cr addition significantly decreased the oxidation mass gain in the heating stage. Higher alloy Al content of 10% further decreased the oxidation mass gain in this initial oxidation stage. The oxidation mass gains of alloys containing 10Al were comparable to those of ternary alloys with 6Al up to 700 °C. The oxidation rates of Fe–Cr–6Al alloys started to increase with further heating, but those of 10Al alloys remained lower, resulting in relatively large difference in oxidation mass gains between the alloys with 6 and 10Al after heating to 1000 °C. Among the alloys with 6Al, oxidation mass gain after heating to 1000 °C was higher for 24Cr than for 4Cr, whereas no such difference in oxidation mass gain was observed between Fe–10Al alloys with different Cr contents.

This tendency of Cr effect on oxidation mass gain is clearly seen in Fig. 3a–c. After heating to 650 °C, the oxidation mass gain of 6Al alloys was drastically decreased by only 4%Cr addition and gradually decreased with further Cr addition. However, after heating to higher temperatures, 900 and 1000 °C, higher Cr addition resulted in an increase in the oxidation mass gain. In the case of 10Al alloys, the oxidation mass gain tended to decrease with higher Cr addition at all temperatures.

In Situ High-Temperature X-Ray Diffraction Measurement

Figure 4 shows the in situ high-temperature X-ray diffraction patterns of Fe–4Cr–6Al, Fe–24Cr–6Al, Fe–4Cr–10Al and Fe–24Cr–10Al during heating to 1000 °C, followed by isothermal oxidation for 20 min. The diffraction patterns of Fe–4Cr–6Al and Fe–24Cr–6Al are also shown from our previous study [5] for further discussion of the development of Al_2O_3 scale. Fe-rich transient oxide, Fe_2O_3, was always observed initially even on the alloys with higher Al content (see Fig. 4e–h). As we previously discussed [5], the peak position of this transient Fe_2O_3 formed on Fe–4Cr–6Al alloy shifted toward lower 2θ position during heating, whereas it shifted opposite direction, i.e., toward higher angles on Fe–24Cr–6Al. In the case of alloys containing higher Al content, the peak position of the transient Fe_2O_3 shifted to higher 2θ position regardless of Cr content. The diffracted signal from α-Al_2O_3 was observed on all alloys during heating. Intensity of signals from Fe_2O_3 suddenly increased when the signals α-Al_2O_3 were observed.

Figure 5 shows the change in signal intensity of different oxides formed during heating to 1000 °C followed by isothermal oxidation for 20 min. The diffracted signals from α-Al_2O_3 were initially observed on all alloys when the sample temperature reached about 900 °C. The time to observation of the signals from α-Al_2O_3 tended to be earlier for the alloys with higher Al content, suggesting higher
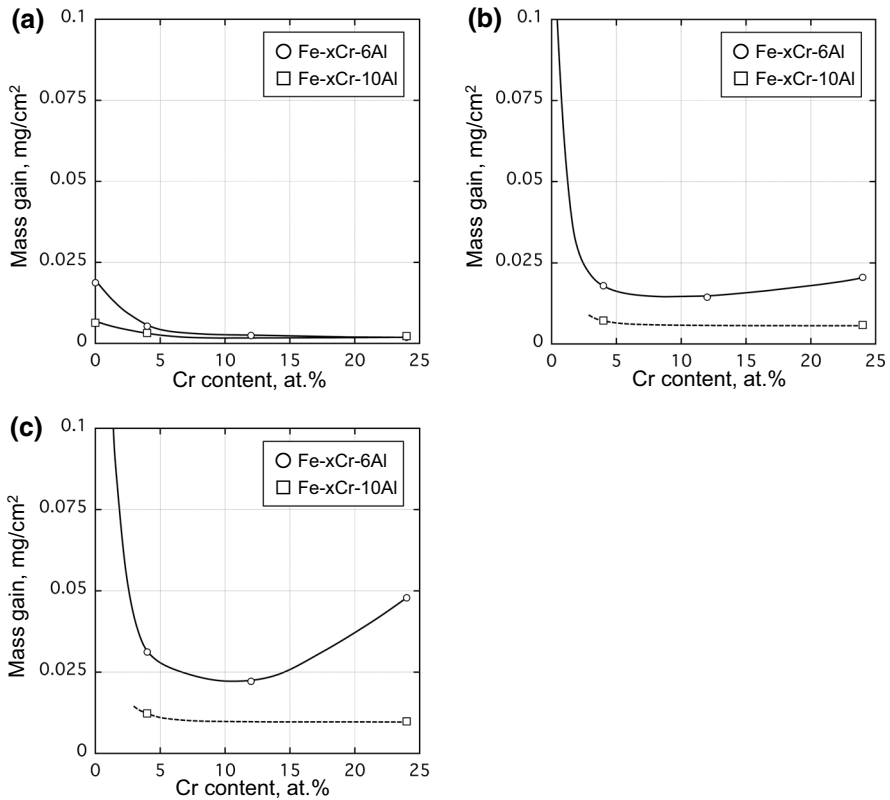
Fig. 3 Change in mass gain with alloy Cr content after heating to different temperature **a** 650 °C, **b** 900 °C and **c** 1000 °C

Al content is beneficial for rapid establishment of α-Al$_2$O$_3$. The intensity of the signals from Fe$_2$O$_3$ suddenly increased concurrently with the formation of α-Al$_2$O$_3$ on the alloys with 6Al, and then it gradually decreased after longer oxidation time due to the formation and growth of (Fe,Cr)$_2$O$_3$ solid solution. However, the signals from transient oxides formed on 10Al alloys disappeared shortly after Al$_2$O$_3$ formation. On the alloys with higher Al content, intensity of the signal from α-Al$_2$O$_3$ gradually increased with temperature and/or time. Additional signals from α-Al$_2$O$_3$ which have different 2-theta angles were observed on all alloys except Fe–4Cr–6Al during isothermal oxidation.

Change in the d-spacing and the full width at half maximum, FWHM, obtained from the signal of Al$_2$O$_3$ (104) are shown in Fig. 6. The d-spacing of Al$_2$O$_3$, which formed initially on alloys with low Al content, was similar and close to that of pure Al$_2$O$_3$ [7, 8] (Fig. 6a). However, on the alloys with higher Al content, the d-spacing of initially formed Al$_2$O$_3$ was larger than that of pure Al$_2$O$_3$ and gradually decreased with oxidation time. The secondary Al$_2$O$_3$ formed on Fe–24Cr–6Al alloy had larger d-spacing, but that formed on 10Al alloys was smaller and similar to pure Al$_2$O$_3$. The FWHM of Al$_2$O$_3$ was higher when the Al$_2$O$_3$ has larger d-spacing.
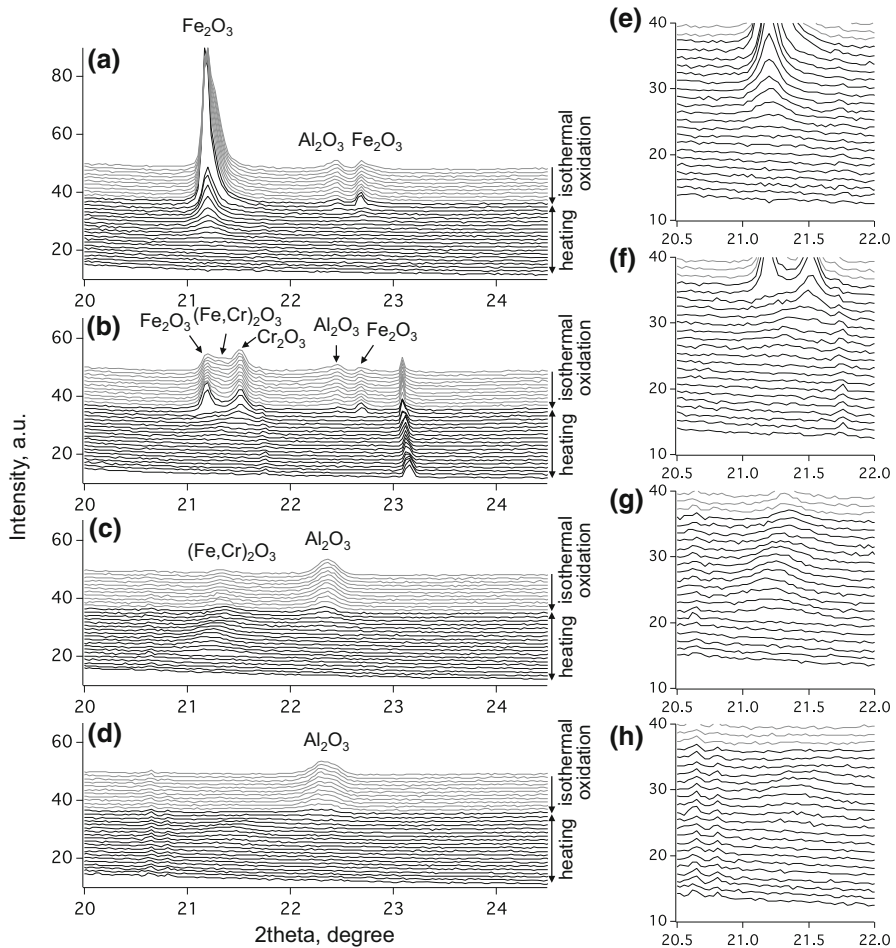
Fig. 4 In situ high-temperature X-ray diffraction pattern of **a**, **e** Fe–4Cr–6Al, **b**, **f** Fe–24Cr–6Al, **c**, **g** Fe–4Cr–10Al and **d**, **h** Fe–24Cr–10Al. The data of Fe–4Cr–6Al and Fe–12Cr–6Al are superimposed from Fig. 3 in Ref. [5]

Change in Microstructure of Oxide Scale During Heating to 1000 °C

Figure 7 shows cross sections of Fe–24Cr–6Al after heating to 800, 900 and 1000 °C. As discussed in our previous study, the Al in low Al alloys oxidized internally, even though the Cr content was high, 24Cr. The internal oxide after heating to 800 °C was identified in this study as an Al_2O_3 by STEM–EDS as shown in Table 2 and was also confirmed to be amorphous due to the absence of diffracted signals from α-Al_2O_3 from both in situ high-temperature XRD measurement and TEM observation. The amorphous internal Al_2O_3 precipitates transitioned to crystalline Al_2O_3 at about 900 °C, and the crystalline Al_2O_3 precipitates grew larger with time and temperature during heating, finally connecting with each other to
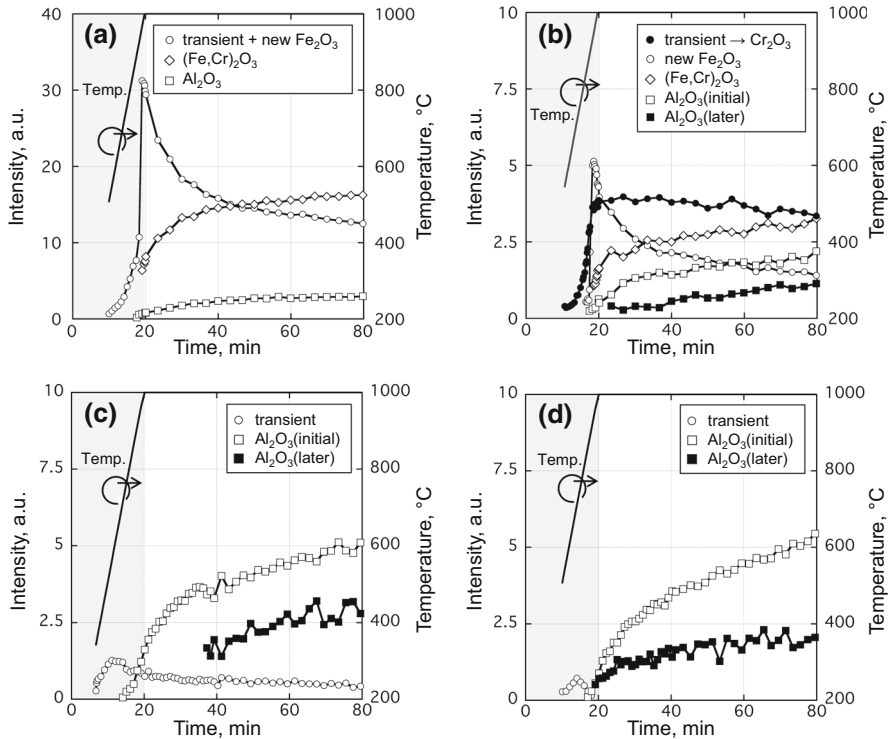
Fig. 5 Change in intensity of different oxide phases on **a** Fe–4Cr–6Al, **b** Fe–24Cr–6Al, **c** Fe–4Cr–10Al and **d** Fe–24Cr–10Al with temperature and/or oxidation time obtained from the XRD patterns in Fig. 4

form an external Al_2O_3 scale below the transient oxide after heating to 1000 °C. STEM–EDS analysis revealed that Fe and Cr contents in the Al_2O_3 precipitates formed after heating to 1000 °C were very low as shown in Table 2. After the formation of internal Al_2O_3 precipitates at 800 °C, the Al-rich amorphous oxide layer disappeared (see Fig. 7a). Figure 8 shows cross sections of Fe–4Cr–6Al after heating to 800 and 900 °C. The volume fraction of Al_2O_3 internal precipitates in this alloy was smaller than that in Fe–24Cr–6Al.

Figure 9 shows cross sections of Fe–4Cr–10Al after heating to 700, 900 and 1000 °C, and Fe–24Cr–10Al after heating to 1000 °C. Because the microstructures of oxide scale formed on Fe–4Cr–10Al and Fe–24Cr–10Al at 1000 °C are almost identical, as shown in Fig. 10c, d, Fe–4Cr–10Al alloy will be the focus of further discussion. A thin Al-rich amorphous oxide layer, which was seen as a bright contrast layer, was observed below the transient Fe_2O_3 layer after heating to 700 °C. Although the interface between outer crystalline transient Fe_2O_3 and inner amorphous Al-rich oxide layer was not clear, the region of crystallinity was clearly seen to increase in the outer part of the amorphous layer with increasing oxidation temperature. When the temperature reached 1000 °C, the Al-rich amorphous oxide layer had become completely crystalline. STEM–EDS analysis of oxide scales after heating to 1000 °C, shown in Figs. 10, 11 and Tables 3 and 4, revealed that the
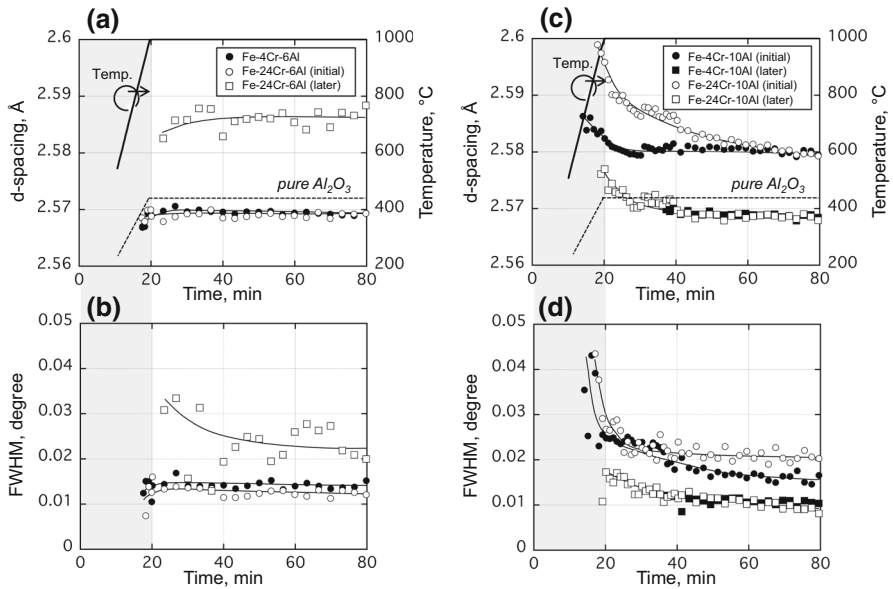
Fig. 6 Change in d-spacing and FWHM of Al_2O_3 on **a**, **b** Fe-4, 24Cr–6Al, **c**, **d** Fe-4, 24Cr–10Al with temperature and/or oxidation time obtained from the XRD patterns in Fig. 4

oxide scale formed on both alloys consisted of Al_2O_3 with much higher Fe and/or Cr contents in the outer part of the scale, and lower Fe and/or Cr contents in the inner part of the scale.

Discussion

Diffracted signals from Al_2O_3 were initially observed during heating on all alloys, and the time to detection of the signals from Al_2O_3 tended to be shorter for alloys with high Al content. An Al-rich amorphous oxide layer developed on all alloys and remained up to about 800 °C, but it broke down, and internal Al_2O_3 was formed in alloys with low Al content. However, the Al-rich amorphous layer transitioned to an external Al_2O_3 scale without internal precipitates on alloys containing higher Al content.

The mass gain during heating was small on all alloys regardless of composition of the transient oxide. This smaller mass gain was interpreted in our previous study to be due to suppression of outward diffusion flux of Fe and Cr by the Al-rich amorphous layer. Moreover, the difference in mass gain during heating before and after Al_2O_3 establishment was small, indicating that the transition from an Al-rich amorphous oxide layer at lower temperatures to formation of a protective Al_2O_3 scale proceeded quickly. However, different oxidation kinetics of Fe–xCr–6Al and Fe–xCr–10Al before and after formation of Al_2O_3 indicates that formation behavior of the external Al_2O_3 scale on alloys with different Al contents is not identical.
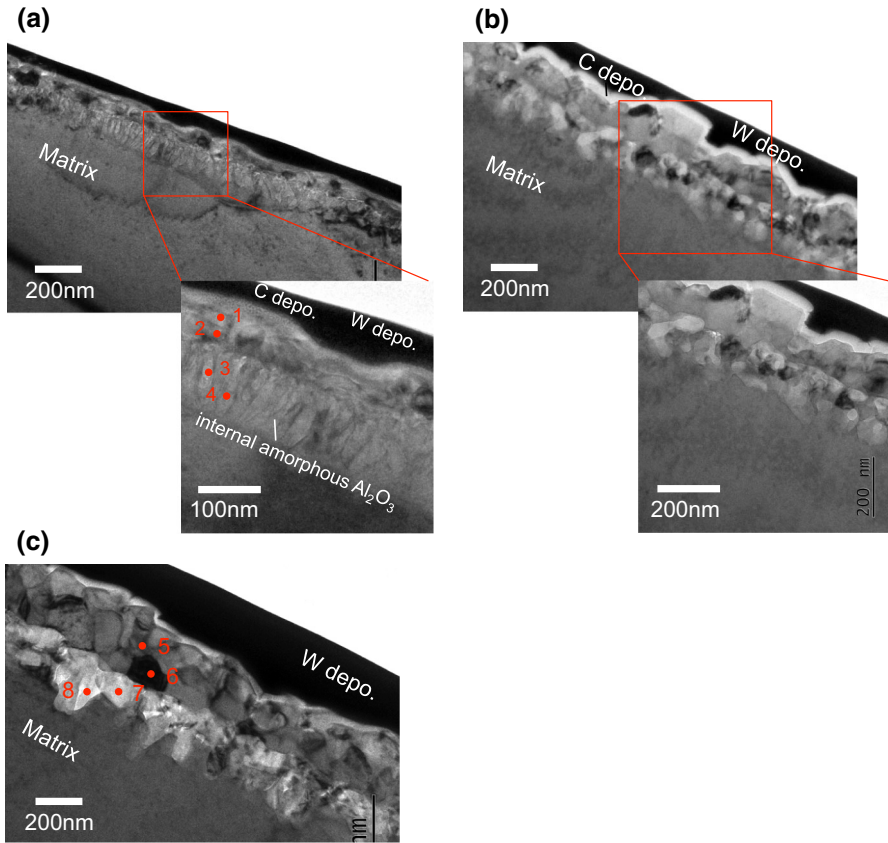
Fig. 7 TEM cross sections of Fe–24Cr–6Al after heating to **a** 800 °C, **b** 900 °C and **c** 1000 °C. Points in **a** and **c** are analysis points by EDS in Table 2

Table 2 STEM–EDS point analysis of Fe–24Cr–6Al after heating to 800 and 1000 °C

	Fe (at.%)	Cr (at.%)	Al (at.%)	O (at.%)
1	58.4	26.6	0.5	14.5
2	60.5	28.3	1.8	14.5
3	51.6	12.7	20.7	15.0
4	35.2	9.5	27.2	28.2
5	0.7	53.4	0.2	45.8
6	76.1	23.3	0.3	1.3
7	0.5	0.2	42.2	57.0
8	0.8	0.5	43.5	55.2

Analysis points are indicated in Fig. 7
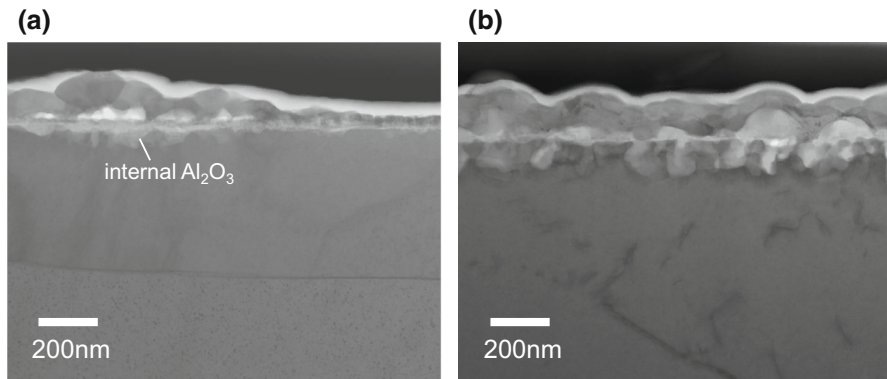
Fig. 8 TEM cross sections of Fe–4Cr–6Al after heating to **a** 800 °C, **b** 900 °C

The Transition and Formation Behavior of the External Al_2O_3 Scale on Alloys with Low Al Content

As shown in Fig. 7, internal Al_2O_3 precipitates were developed below an Al-rich amorphous oxide layer in the low Al alloy. It was found that a continuous Al_2O_3 scale was established by connecting internal Al_2O_3 precipitates due to lateral growth of those precipitates with increasing temperature. The internal Al_2O_3 precipitates were amorphous when they formed initially. Although formation of the amorphous internal oxide has not been reported previously in the literature, it is reasonable to consider that an amorphous structure is favorable for reduction in interfacial energy at the interface between the precipitates and the substrate. With increase in temperature to about 900 °C, those internal Al_2O_3 precipitates became stable crystalline α-Al_2O_3, which has similar d-spacing to pure Al_2O_3. EDS analysis also revealed that Fe and/or Cr contents in the precipitates are very low. Additional peaks from Al_2O_3, which had larger d-spacing and FWHM, were detected during isothermal oxidation on Fe–24Cr–6Al. This result implies that the initially formed Al_2O_3 precipitates reacted with the outer Cr-rich transient oxide of $(Cr, Fe)_2O_3$ and/or Fe_2O_3 to form a solid-solution of $(Al,Fe,Cr)_2O_3$.

Figure 12a shows the change in thickness of both the outer oxide scale and internal oxidation zone during heating from 800 to 1000 °C on Fe–24Cr–6Al. The thickness of the outer oxide increased rapidly within this temperature range because of physical breakdown of the amorphous layer due to deformation of alloy substrate accompanied with the formation of internal Al_2O_3 precipitates [6]. However, the overall oxidation mass gain of this alloy was still much lower than that of Fe–6Al as shown in Fig. 2, indicating that the transition from internal Al_2O_3 to a continuous Al_2O_3 scale proceeds rapidly after destruction of the Al-rich amorphous layer. In comparison with the outer oxide scale, the increase in thickness of the internal oxidation zone from 800 to 900 °C is smaller, but the volume fraction of internal Al_2O_3 increased in this temperature range (Fig. 12c). Moreover, the number of internal Al_2O_3 precipitates per unit surface length decreased with increasing temperature. These results indicate that lateral growth of internal Al_2O_3 precipitates
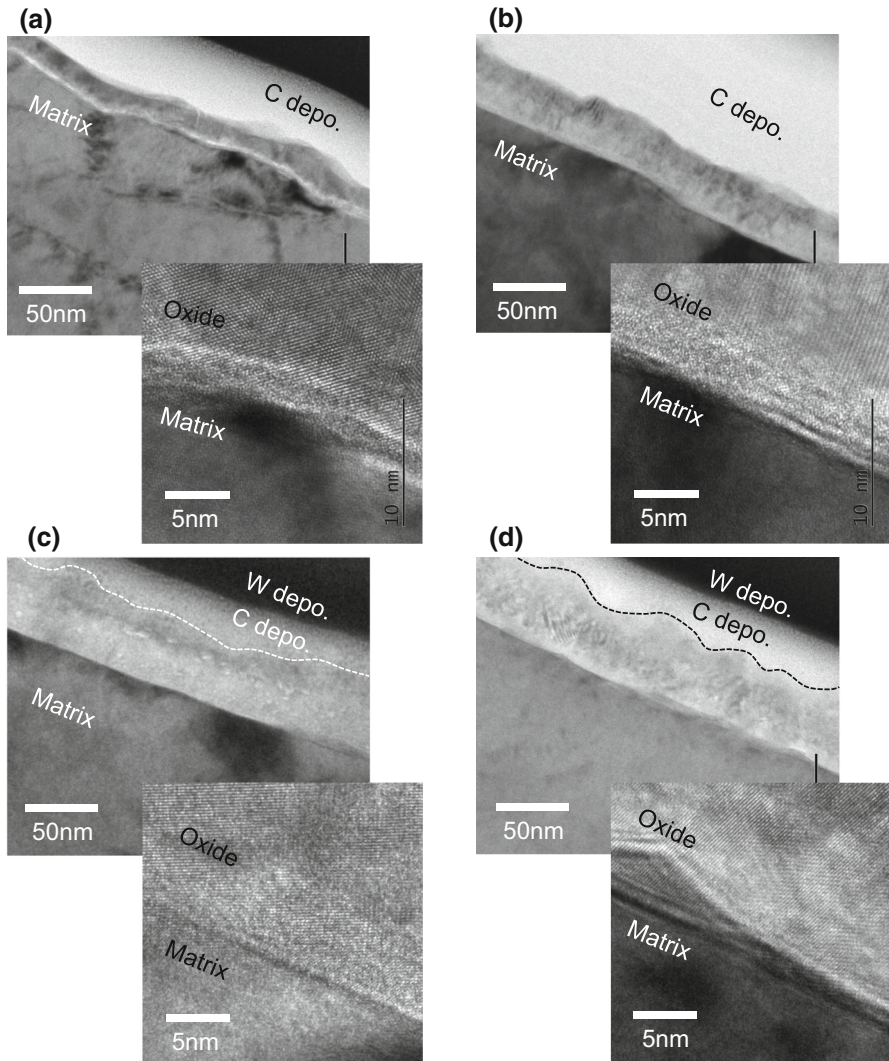
Fig. 9 TEM cross sections after heating to **a** 700 °C, **b** 900 °C, **c** 1000 °C on Fe–4Cr–10Al and **d** 1000 °C on Fe–24Cr–10Al

predominated, and this lateral growth of internal Al_2O_3 precipitates promoted the establishment of an external Al_2O_3 scale. Therefore, higher alloy Cr content and a higher volume fraction of internal Al_2O_3 precipitates are favorable for rapid establishment of an external Al_2O_3 scale.
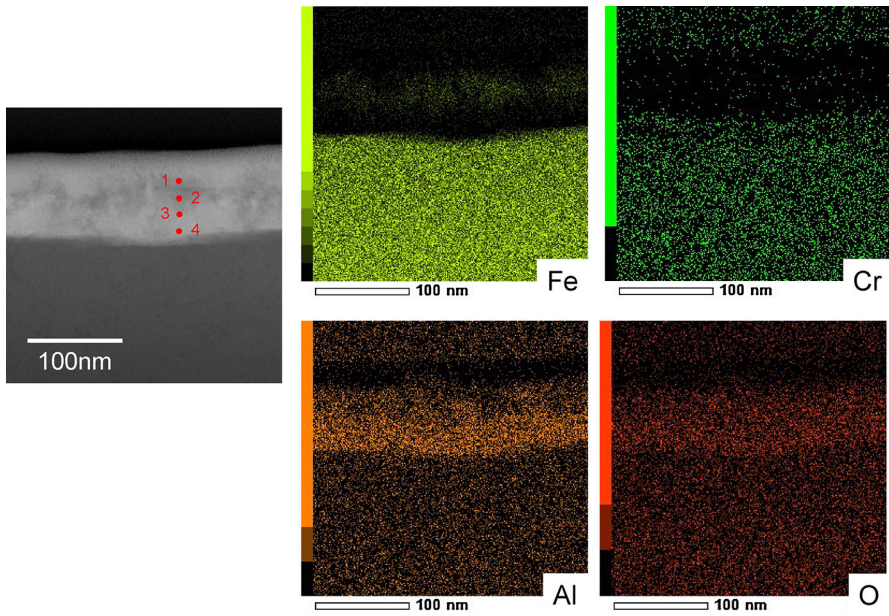
Fig. 10 STEM–EDS mapping of Fe–4Cr–10Al after heating to 1000 °C. Points are analysis points by EDS in Table 3
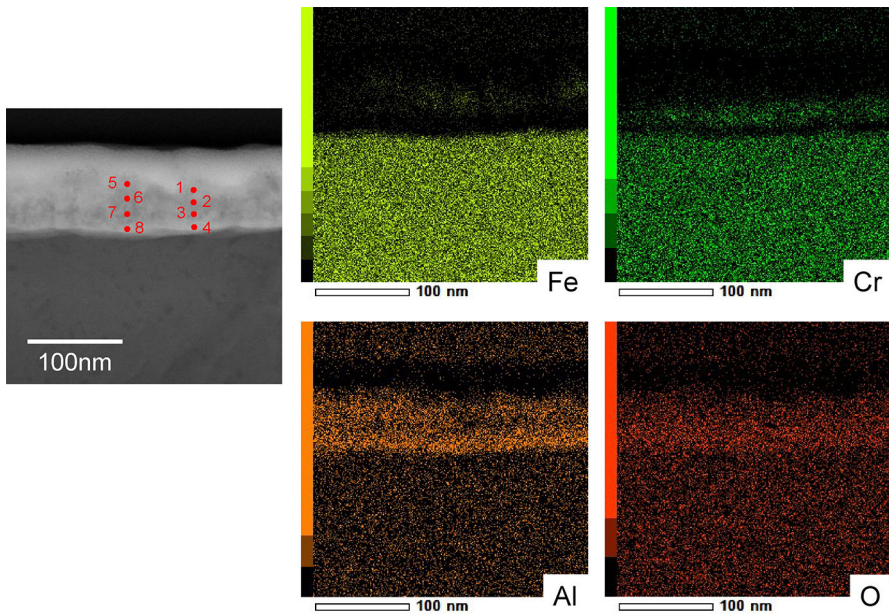

Fig. 11 STEM–EDS mapping of Fe–24Cr–10Al after heating to 1000 °C. Points are analysis points by EDS in Table 4

Table 3 STEM–EDS point analysis of Fe–4Cr–10Al after heating to 1000 °C

	Fe (at.%)	Cr (at.%)	Al (at.%)	O (at.%)
1	42.4	0.4	17.8	39.5
2	38.3	0.0	21.1	40.6
3	5.2	0.7	43.0	51.0
4	2.5	4.6	39.2	53.7

Analysis points are indicated in Fig. 10

Table 4 STEM–EDS point analysis of Fe–24Cr–10Al after heating to 1000 °C

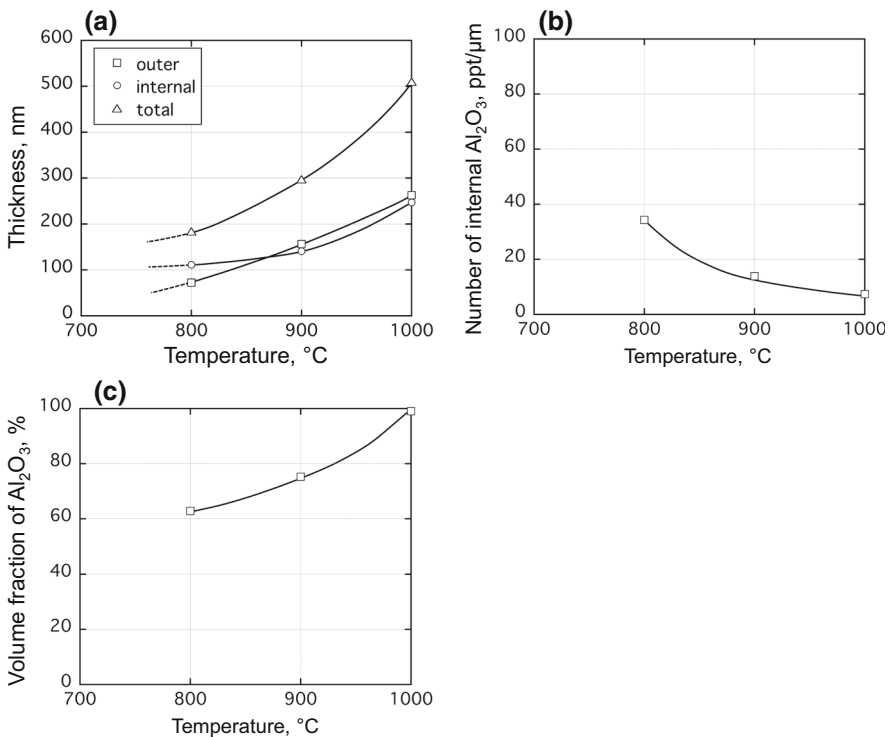|	Fe (at.%)	Cr (at.%)	Al (at.%)	O (at.%)
1	6.1	1.6	43.4	48.9
2	10.4	5.0	34.9	49.8
3	8.6	22.6	24.5	44.4
4	0.9	0.9	45.7	52.5
5	32.8	4.3	25.3	37.6
6	20.2	3.6	33.7	42.5
7	5.8	16.7	30.7	46.8
8	1.4	1.4	45.1	52.1

Analysis points are indicated in Fig. 11

Fig. 12 a Change in the thickness of the outer transient oxide and IOZ or inner Al_2O_3 during heating, change in **b** number, **c** volume fraction of Al_2O_3 during heating of Fe–24Cr–6Al

The Transition and Formation Behavior of External Al$_2$O$_3$ Scale on the Alloy with High Al Content

As shown in Fig. 9, internal Al$_2$O$_3$ precipitates were not formed in the alloys with higher Al content. An Al-rich amorphous layer transformed to crystalline from the outer (transient oxide side) to the inner part of the amorphous layer during heating. Greater Al supply from the alloy substrate to the Al-rich amorphous layer in alloys with high Al content prevents formation of internal Al$_2$O$_3$ precipitates below the amorphous layer, resulting in a longer lifetime for the Al-rich amorphous layer. The transient oxide formed at the initial stage of oxidation was always of corundum-type (Fe,Cr)$_2$O$_3$, which is of similar crystallographic structure to α-Al$_2$O$_3$. Such initial transient oxide scale formation is known to promote the rapid transformation to α-Al$_2$O$_3$, or to suppress metastable Al$_2$O$_3$ formation [3, 9]. This "template effect" could also promote the amorphous to crystalline transformation.

The in situ high-temperature X-ray diffraction measurement clearly showed that the α-Al$_2$O$_3$, formed initially on alloys with higher Al content, had larger d-spacing and FWHM, because the α-Al$_2$O$_3$ contained higher Fe and/or Cr contents. This Al$_2$O$_3$, which has larger d-spacing, was reported on Fe–high Al binary alloys [10, 11]. Cr$_2$O$_3$ and Al$_2$O$_3$ form a solid-solution [12], but solubility of Fe$_2$O$_3$ in Al$_2$O$_3$ is relatively small, 5.3 mol% at 1000 °C [13], thus the d-spacing of initially formed α-Al$_2$O$_3$ on higher Cr alloys could be larger than that formed on a lower Cr alloy.

The Effect Cr and Al on the Transition Behavior of External Al$_2$O$_3$ Scale

Figure 13 shows schematics of the effect of Cr and Al on the transition to external Al$_2$O$_3$ scale. Cr content had little effect on the transition to an external Al$_2$O$_3$ scale on alloys with higher Al content, but Al content was found to strongly affect this transition. Internal Al$_2$O$_3$ precipitates were developed in 6%Al alloys regardless of Cr content; however, internal Al$_2$O$_3$ was not formed when Al was increased to 10%. This result suggests that the "true" critical Al content for external Al$_2$O$_3$ scale formation exists between 6–10% on Fe–Cr–Al at 1000 °C. Cr content seems not to significantly affect this critical Al content, but helps to promote establishment of an external Al$_2$O$_3$ scale when Al content is below the critical value.

An increase in volume fraction of internal Al$_2$O$_3$ resulted in fast establishment of Al$_2$O$_3$ scale, as presented in our previous paper [5]. Since the volume fraction of internal Al$_2$O$_3$ increases with increasing alloy Cr content, Cr should help to promote Al$_2$O$_3$ scale formation by accelerating the transition from internal to external scale formation; therefore, Cr is important mostly on the alloys with lower Al content. However, if the Al-rich amorphous layer directly transitions to an external Al$_2$O$_3$ scale, the Cr effect on external Al$_2$O$_3$ scale formation is greatly diminished.
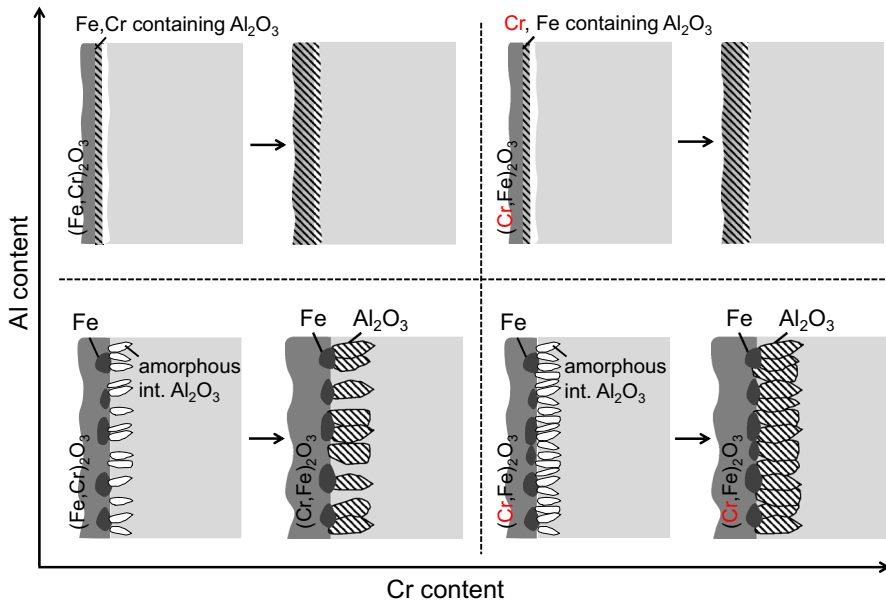
Fig. 13 Schematics of the effect of Cr and Al on the transition from transient oxides to external Al_2O_3 scale

Conclusions

The transition behavior from Al-rich amorphous oxide to external Al_2O_3 layer was investigated by structural and microstructural observation in the heating stage by means of in situ high-temperature X-ray diffraction measurement and TEM. The results obtained may be summarized as follows:

1. Internal Al_2O_3 precipitates formed in 6Al alloys grew laterally and connected with each other to form an external Al_2O_3 scale. The Al_2O_3 scale developed by this pathway contained low Fe and Cr contents.
2. Al-rich amorphous layer became crystalline from the outer toward the inner part of the layer with increasing temperature and time, and then external Al_2O_3 was finally developed on alloys with high Al content. Al_2O_3 scale formed by this pathway contained higher Fe and Cr content.
3. Cr promoted the Al_2O_3 scale formation by increasing the volume fraction of internal Al_2O_3 on alloys with lower Al content; however, no significant effect of Cr on Al_2O_3 scale formation was observed on alloys with higher Al content, if the amorphous layer directly transitioned to Al_2O_3 scale.

References

1. F. A. Golightly, G. C. Wood and F. H. Stott, *Oxidation of Metals* **14**, 217 (1980).
2. B. H. Kear, L. P. Lemaire, D. E. Fornwalt and F. S. Pettit, *Oxidation of Metals* **3**, 557 (1971).
3. M. W. Brumm and H. J. Grabke, *Corrosion Science* **33**, 1677 (1992).
4. Y. Kitajima, S. Hayashi, T. Nishimoto, T. Narita and S. Ukai, *Oxidation of Metals* **73**, 375 (2010).
5. S. Yoneda, S. Hayashi, I. Saeki and S. Ukai, *Oxidation of Metals* **86**, 357 (2016).
6. S. Yoneda, S. Hayashi and S. Ukai, *Oxidation of Metals* (2017). doi:10.1007/s11085-017-9761-1.
7. T. Fujimura and S.-I. Tanaka, *Journal of Materials Science* **34**, 425 (1999).
8. I. E. Reimanis, K. P. Trumble, K. A. Rogers and B. J. Dalgleish, *Journal of the American Ceramic Society* **80**, 424 (1997).
9. D. Renusch, M. Grimsditch, I. Koshelev, B. W. Veal and P. Y. Hou, *Oxidation of Metals* **48**, 471 (1997).
10. S. Hayashi, I. Saeki, Y. Nishiyama, T. Doi, S. Kyo and M. Segawa, *Materials Science Forum* **696**, 63 (2011).
11. S. Hayashi, Y. Takada, I. Saeki, A. Yamauchi, Y. Nishiyama, T. Doi, S. Kyo and M. Sato, *Materials and Corrosion* **63**, 862 (2012).
12. M. Fujita, K. Inukai, S. Sakida, T. Nanba, J. Ommyoji, A. Yamaguchi and Y. Miura, *Journal of the Society of Materials Science* **56**, 526 (2007).
13. F. A. Elrefaie and W. W. Smeltzer, *Metallurgical Transactions B* **14B**, 85 (1983).